ARTICLES
PUBLISHED ONLINE: 22 FEBRUARY 2016 | DOI: 10.1038/NCHEM.2462
nature chemistry

Encoding complexity within supramolecular analogues of frustrated magnets

Andrew B. Cairns[1,2], Matthew J. Cliffe[1,3], Joseph A. M. Paddison[1,4,5], Dominik Daisenberger[6], Matthew G. Tucker[4,6], François-Xavier Coudert[7]* and Andrew L. Goodwin[1]*

The solid phases of gold(I) and/or silver(I) cyanides are supramolecular assemblies of inorganic polymer chains in which the key structural degrees of freedom—namely, the relative vertical shifts of neighbouring chains—are mathematically equivalent to the phase angles of rotating planar ('XY') spins. Here, we show how the supramolecular interactions between chains can be tuned to mimic different magnetic interactions. In this way, the structures of gold(I) and/or silver(I) cyanides reflect the phase behaviour of triangular XY magnets. Complex magnetic states predicted for this family of magnets—including collective spin-vortices of relevance to data storage applications—are realized in the structural chemistry of these cyanide polymers. Our results demonstrate how chemically simple inorganic materials can behave as structural analogues of otherwise inaccessible 'toy' spin models and also how the theoretical understanding of those models allows control over collective ('emergent') phenomena in supramolecular systems.

At the heart of systems chemistry lies the idea that supramolecular interactions can give rise to complex and unexpected collective states that emerge on a fundamentally different length scale to that of the interactions themselves[1,2]. In certain cases—for example, the self-assembly of virus-like polyhedral cages from coordination building blocks[3]—it is possible to control emergence in a systematic manner, but the development of general approaches remains a fundamental challenge in the field[4]. In the conceptually related domain of frustrated magnetism, where collective states give rise to exotic physics of relevance to data storage and spintronics, the task of predicting emergent behaviour is simplified through control over the geometry and form of the magnetic interactions from which complexity arises[5]. Seeking to combine approaches from these two fields, we study here the solid phases of coordination polymer chains assembled from non-magnetic gold(I) and/or silver(I) cations and cyanide anions. We proceed to show how the periodic inter-chain potential encodes a supramolecular interaction that can be tuned to mimic different magnetic interactions between XY spins (that is, spins confined to lie in a single plane, also termed 'spin rotors'). Because the chains pack on a triangular lattice, the crystal structures of gold(I) and/or silver(I) cyanides can then be interpreted in terms of the phase behaviour of magnets in which XY spins are also arranged on a triangular lattice (so-called 'triangular XY' magnets)[6].

The existence of conceptual mappings between complex magnetic and structural states of matter has long been appreciated[7]. Arguably the most famous example is the low-temperature magnetic state of 'spin ice' $Ho_2Ti_2O_7$ (ref. 8), in which tetrahedral spin clusters adopt a 'two-in–two-out' arrangement geometrically related to the orientation of water molecules in cubic ice[9]. This mapping results in the same characteristically large configurational entropy for both systems[10] and even relates their excitations: the magnetic 'monopoles' of spin ices and the Bjerrum H_3O^+/OH^- pairs in ice are different manifestations of the same geometric defect[11]. Ice-like states are just one example of complex matter and much of the field of frustrated magnetism is concerned with the extraordinary diversity of phases accessible through different combinations of lattice geometries, pairwise interactions and effective degrees of freedom[12]. As in systems chemistry, the interest is very often in collective ('emergent') states where a system develops order on new length scales or evolves new degrees of freedom distinct from those of the individual components[13]. This interest is not only academic: the magnetic vortices present in the so-called skyrmion phase of chiral ferromagnets offer a possible mechanism of ultra-dense data storage[14], and the spin-ice magnetic monopoles may yet be exploited in the emerging field of 'magnetronics'[15].

A natural question is whether structural analogues of frustrated magnets might explore the same diversity of phase behaviour, perhaps allowing the physical realization of systems that are difficult to access when considering magnetic interactions alone. For example, there are few magnetic systems that are strictly two-dimensional in nature, because some degree of interaction in a perpendicular direction usually persists[16]. Supramolecular analogues offer a neat solution to this problem: one-dimensional polymers can behave as single collective objects, such that the interactions between them are strictly two-dimensional. In this way, aggregates of polar polymer chains have provided some of the first physical realizations of the canonical triangular and square Ising models (two-dimensional systems with binary degrees of freedom, for example, spin-up/spin-down)[17–19] and have been used to generate complex collective states based on geometric frustration[20]. Other aspects of mapping between magnetic and structural states may prove more difficult to achieve. By their very nature, non-magnetic systems lend themselves most naturally to discrete degrees of freedom—for example, the switching of charge states, atom positions or orbital orientations[7,21–23]. Consequently, it is not yet clear that meaningful structural analogues exist for many of the complex magnetic phases that can arise when spins possess continuous degrees of freedom[24].

[1]Department of Chemistry, University of Oxford, Inorganic Chemistry Laboratory, South Parks Road, Oxford, OX1 3QR, UK. [2]European Synchrotron Radiation Facility, 71 avenue des Martyrs, 38043 Grenoble, France. [3]Department of Chemistry, University of Cambridge, Lensfield Road, Cambridge CB2 1EW, UK. [4]ISIS Facility, Rutherford Appleton Laboratory, Harwell Oxford, Didcot, OX11 0QX, UK. [5]School of Physics, Georgia Institute of Technology, 837 State Street, Atlanta, Georgia 30332, USA. [6]Diamond Light Source, Chilton, OX11 0DE, UK. [7]PSL Research University, Chimie ParisTech – CNRS, Institut de Recherche de Chimie Paris, 75005 Paris, France. *e-mail: fx.coudert@chimie-paristech.fr; andrew.goodwin@chem.ox.ac.uk

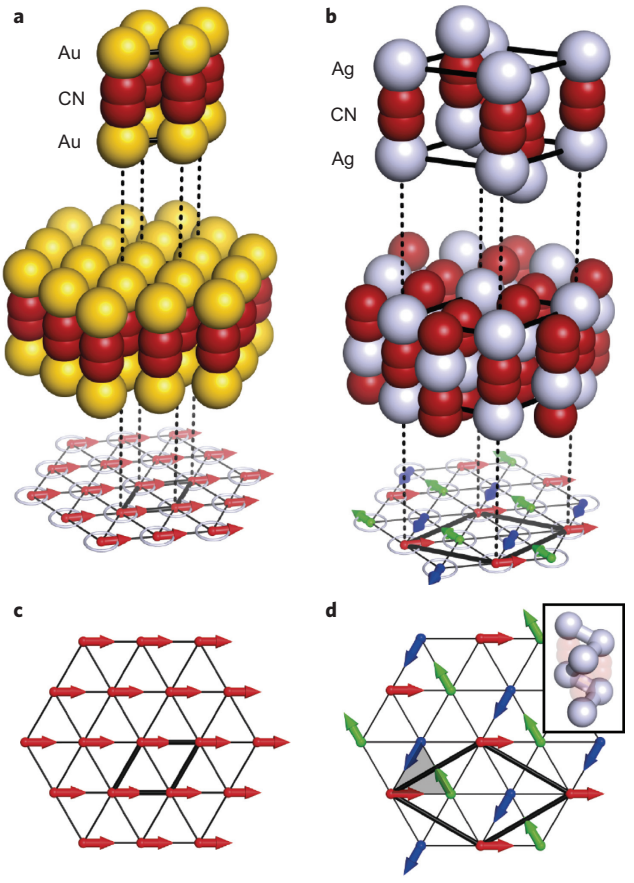

Figure 1 | Crystal structures of AuCN and AgCN and their relationship to the ground states of triangular XY (anti)ferromagnets. a,**b**, The crystal structures of both AuCN (**a**) and AgCN (**b**) consist of one-dimensional metal–cyanide chains arranged on a triangular lattice. The structures differ in the relative heights of neighbouring chains. In AuCN, the metal atoms (large gold spheres) form close-packed planes; this arrangement has *P6/mmm* symmetry. In AgCN, neighbouring chains are displaced by 1/3 of the chain repeat to bring the metal cations (large silver spheres) closer to the cyanide anions (smaller red spheres). This structure has a larger unit cell with $R\bar{3}m$ symmetry. The relative height of each chain can be represented by a phase angle, shown here projected onto the underlying triangular lattice. The arrows that represent these phase angles are coloured according to their orientation. **c**,**d**, The magnetic ground states of the triangular XY ferromagnet (**c**) and antiferromagnet (**d**) correspond to this interpretation of the structures of AuCN and AgCN. In each case the relevant unit cell is outlined in bold. The chiral degrees of freedom in the 'spin spiral' antiferromagnetic state—given by the sense of spin rotation as the vertices of a triangular plaquette (shaded) are traversed in a common direction—translate to the handedness of argentophilic helices in the AgCN structure (inset in **d**).

Results and discussion

Gold cyanide and silver cyanide. We proceed to establish a mapping between the structural chemistry of gold(I) and/or silver(I) cyanides—compounds usually studied for their unusual thermal expansion behaviour[25–27]—and triangular magnets with continuous (XY) degrees of freedom, but first introduce the crystal structures of AuCN and AgCN themselves. In both cases, the transition-metal cations are coordinated in a linear fashion by two cyanide ions, with each cyanide ion bridging two cations in turn[28]. Contrary to initial reports[29], it is now established that there is no long-range order in the orientation of the cyanide ions for either system, so that both structures consist of essentially the same linear –M–(CN)–M– chains of atoms (here, M = Ag, Au)[25,26]. In each case these chains are arranged on a triangular lattice, but what differs between the two structures is the relative vertical position of neighbouring chains: in AuCN the chains are aligned such that Au^+ cations contact other Au^+ cations, whereas in AgCN there is a successive displacement by 1/3 of the chain repeat length that brings Ag^+ cations closer to CN^- ions than to other Ag^+ cations (Fig. 1a,b). It has been suggested that attractive metallophilic interactions (which are stronger[30–32] for Au^+ than Ag^+) overcome electrostatics in AuCN but not in AgCN, so providing a qualitative understanding of the different structure types adopted[27,33]. By associating the relative vertical position z_j of each M–(CN)–M chain with a phase angle $\theta_j = 2\pi z_j$, we can map these structures onto triangular arrangements of XY spins $\mathbf{S}_j = S(\cos\theta_j, \sin\theta_j)$ of arbitrary magnitude S. In both cases each chain or spin has a single degree of freedom that is periodic in z_j or θ_j, respectively. The spin arrangements corresponding to the AuCN and AgCN structures are shown in Fig. 1c,d; these are well known within the magnetism community as the ground states of the (nearest-neighbour) XY triangular ferromagnet and antiferromagnet, respectively[34]. A simple mapping between collective states in spin and cyanide structures is evident in the latter: the three-spin chiral degrees of freedom that characterize so-called 'spiral order' in the XY triangular antiferromagnet[35] correspond in the AgCN structure to argentophilic helices (Fig. 1d).

Can it be coincidental that these chemically simple transition-metal cyanides adopt structures that map onto the canonical XY triangular magnets? We have already highlighted the relationship that exists between the lattice geometry and effective degrees of freedom in both cases. But to answer this question properly we need to understand how and why the pairwise interactions between neighbouring MCN chains, on the one hand, and neighbouring XY spins, on the other, are also related. To this end, we have used quantum-mechanical calculations to determine the form of the supramolecular interaction potential operating on pairs of neighbouring MCN chains as a function of their relative phase $\Delta\theta = 2\pi\Delta z$ (Fig. 2a). We expect two dominant contributions to this potential, with the particular balance observed depending on the chemistry of the relevant system: metallophilic interactions favour coalignment of chains to minimize M…M separations, whereas electrostatics favour staggering so as to bring the M^+ cations of one chain into registry with the CN^- anions of its neighbour. Our computational results are shown in Fig. 2b, from which it is clear that metallophilicity dominates in the case of AuCN (energy minimum at $\Delta\theta = 0$) but not in the case of AgCN (energy minima at $\Delta\theta = \pm\pi$). Crucially, in both cases, the potentials (E) are well approximated by their first-order Fourier component

$$E = J\cos(\Delta\theta) \quad (1)$$

where the inter-chain coupling parameter J is −7.03(18) kJ mol^{-1} for AuCN and +3.71(5) kJ mol^{-1} for AgCN (Fig. 2b). The similarity to the spin Hamiltonian (H) for the XY triangular (anti)ferromagnet

$$H = J_{XY}\sum_{i,j}\mathbf{S}_i\cdot\mathbf{S}_j = J_{XY}S^2\sum_{i,j}\cos(\Delta\theta_{ij}) \quad (2)$$

is striking (here, i and j index neighbouring spin vectors $\mathbf{S}_i$ and $\mathbf{S}_j$, $S = |\mathbf{S}_i| = |\mathbf{S}_j|$, and $\Delta\theta_{ij}$ describes the angle between the two spin vectors), and suggests that we can understand the structural chemistry of both cyanides in terms of XY spins that interact via an effective nearest-neighbour exchange constant $J_{XY} = J/S^2$. So, for AuCN it is because $J < 0$ that its crystal structure maps onto the ground state of the XY triangular ferromagnet ($J_{XY} < 0$); conversely, the positive value of J for AgCN explains why its structure is related to the

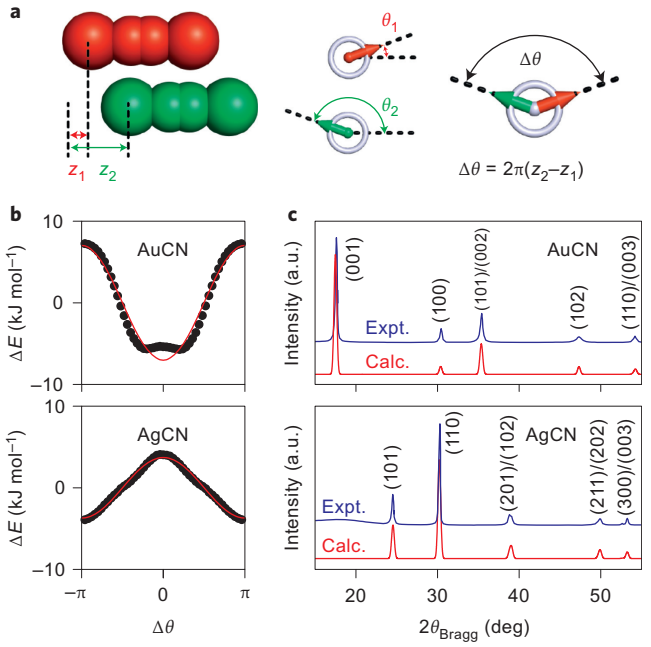

Figure 2 | Interactions in AuCN and AgCN. a, The relative displacement between neighbouring chains, Δz, can be mapped uniquely onto a phase shift $\Delta\theta$ between corresponding XY spins. Here and elsewhere, colour represents phase. **b**, The variation in enthalpy for a pair of AuCN (top) and AgCN (bottom) chains, separated by their respective equilibrium distances, calculated as a function of phase shift $\Delta\theta$. Data are shown as filled circles, and the first-order Fourier component is shown as a red line. **c**, Comparison of experimental[27] and calculated X-ray diffraction patterns (Cu Kα radiation) for AuCN (top) and AgCN (bottom). The structural models used for both calculations were derived from the ground state of the triangular XY magnets to which the relevant energy profile in **b** corresponds. Reflections are indexed according to the corresponding unit cells, which relate, for example, the (100) reflection of AuCN and the (110) reflection of AgCN.

ground state of the XY triangular *anti*ferromagnet. We note that in both cases the effective exchange energies are larger than k_BT under ambient conditions, and orders of magnitude larger than in conventional magnetic systems.

From a supramolecular chemistry perspective, what we are saying is that the self-interaction potentials of AuCN and AgCN chains encode for different collective structures, much as the geometries of coordination chemistry building blocks might encode for differently shaped polyhedral assemblies[3]. For AuCN, energy is minimized by bringing chains into vertical alignment, resulting in the layered structure illustrated in Fig. 1a and the X-ray diffraction pattern shown in Fig. 2c. For AgCN, pairwise interactions are minimized by staggering neighbouring chains by one-half of the chain repeat length. This local arrangement cannot be propagated on the triangular lattice (because one pair of any triplet of neighbouring chains would be forced to adopt the same height); instead, the lowest-energy compromise[34] is for successive heights to differ by $\Delta z = 1/3$, giving the structure represented in Fig. 1b and the X-ray diffraction pattern shown in Fig. 2c. In both cases the higher-order Fourier components to the real interaction potential (Fig. 2b) will influence subtle features of the structures; for example, there is likely to be some buckling of the cation layers in AuCN that arises because the energy minima occur for small but non-zero values of $\Delta\theta$. Nevertheless, the important structural features are clearly captured by the simple model presented here. The mapping onto XY spin systems serves two purposes. On the one hand, it establishes physical realizations of these theoretical spin models, in principle enabling aspects of the models to be tested and studied experimentally. (Note that three-dimensional realizations of triangular magnets generally differ in their behaviour relative to the theoretical two-dimensional case[36].) On the other hand, our understanding of the theory of these magnets allows us to interpret and predict structural features (such as the ground state) of the experimental systems themselves.

Bimetallic silver gold cyanide. Having established a simple mapping for AuCN and AgCN onto the canonical XY triangular magnets, we sought to understand the structural chemistry of the more complex heterometallic phase $Au_{1/2}Ag_{1/2}(CN)$. By way of background, this system is known to adopt a similar triangular rod packing to the homometallic cyanides, with (N-bound) Ag and (C-bound) Au atoms now alternating strictly along any given chain (Fig. 3a)[27]. Despite this local order, the arrangement of chains relative to one another remains uncertain and the true crystal structure is not known[27]. What is clear—both from the experimental data of ref. 27 and our own measurements (Supplementary Discussion 1 and Supplementary Fig. 1)—is that the X-ray diffraction pattern contains regions of structured diffuse scattering that are the signature of the correlated disorder associated with complex states (Fig. 3b)[37]. Our approach to studying this system is as follows: (1) establish, using quantum chemistry methods, the form of the self-interaction potential for Au–CN–Ag–NC–Au chains, (2) determine a mapping onto a suitable XY triangular magnet, and (3) seek to interpret the experimental diffraction pattern of $Au_{1/2}Ag_{1/2}(CN)$ in terms of a structural model determined by analogy to the corresponding magnetic system. In developing this mapping we note the doubled repeat length of Au–CN–Ag–NC–Au chains relative to Au–(CN)–Au and Ag–(CN)–Ag means that the phase shift $\Delta\theta$ adopts a subtly different meaning in this more complicated case. In particular, both $\Delta\theta = 0$ and $\Delta\theta = \pm\pi$ now correspond to situations with strong metallophilic interactions, differing only in whether like ($\Delta\theta = 0$) or unlike ($\Delta\theta = \pm\pi$) atoms are in close contact (Fig. 3a).

Quantum mechanical calculations of the chain self-interaction potential give the trend shown in Fig. 3c. This energy profile is more complex than for the homometallic cyanides, in part because of the Au/Ag alternation and in part because this alternation couples to CN orientations. In simplifying the function $E(\Delta\theta)$, it is now appropriate to consider the first two Fourier components, so as to account for the difference in homometallic versus heterometallic interactions (periodicity $\Delta\theta = 2\pi$) as well as the difference in average metallophilic and electrostatic interactions (each with periodicity $\Delta\theta = \pi$):

$$E = J_1\cos(\Delta\theta) + J_2\cos(2\Delta\theta) \quad (3)$$

$$\equiv J_1\cos(\Delta\theta) + J_2\cos^2(\Delta\theta) \quad (4)$$

This approximation is poorest at the highest-energy region of the interaction potential, but accounts reasonably well for the overall shape near the energy minimum, the more critical feature (Fig. 3c). Our data give $J_1 = +2.3(3)$ kJ mol^{-1} and $J_2 = -1.3(5)$ kJ mol^{-1}. The J_2 term describes the difference in average metallophilic and electrostatic interactions, and its small value demonstrates the especially delicate balance between these two terms in this case—unsurprising, of course, given the different structures of AgCN and AuCN themselves. Instead the dominant interaction in equation (4) is described by the J_1 term; its positive value corresponds to a preference for heterometallic Ag…Au contacts relative to a combination of homometallic Ag…Ag and Au…Au contacts.

The relevant magnetic system is now the so-called bilinear–biquadratic (BLBQ) XY model, characterized by the spin Hamiltonian

$$H = J_1 \sum_{i,j} \mathbf{S}_i \cdot \mathbf{S}_j + J_2 \sum_{i,j} \left| \mathbf{S}_i \cdot \mathbf{S}_j \right|^2 \quad (5)$$

$$= J_1 \sum_{i,j} \cos(\Delta\theta_{ij}) + J_2 \sum_{i,j} \cos^2(\Delta\theta_{ij}) \quad (6)$$

where we have subsumed the dependency on spin magnitude S within the J_n. In practice, the BLBQ model is most frequently used to describe $S = 1$ systems[38,39], with J_1 and J_2 terms quantifying the strength and nature of dipolar and quadrupolar interactions, respectively. For XY spins, the thermodynamic phase diagram is known from theory[6]; the particular combination of J_1, J_2 values determined above corresponds to a complex 'nematic' ground state in which dipolar disorder is coupled with (hidden) ferroquadrupolar order (Fig. 3d). In other words, neighbouring spins align along a common axis but their absolute orientations—though more frequently antiparallel than parallel—are not ordered. To the best of our knowledge, this state has never been realized in a physical system[16,36,40]. The implication for the structure of $Au_{1/2}Ag_{1/2}(CN)$ is that chains should align to bring metal cations in registry with one another, with a preference for unlike Ag…Au neighbours. This arrangement is geometrically frustrated (because any triplet of neighbouring Au/Ag atoms must contain at least one pair of like atoms) and would represent a disordered state related to the two ordered candidate structures proposed in ref. 27 on the basis of their fits to neutron pair distribution functions (Supplementary Fig. 2). The X-ray diffraction pattern calculated for a structural model of $Au_{1/2}Ag_{1/2}(CN)$ based on this strict quadrupolar order is shown in Fig. 3b. Although the general intensity distribution and reflection conditions of the diffraction pattern are reproduced, the degree of diffuse scattering and selective peak broadening is underestimated. (Note that equivalent calculations based on the other phases described by the J_1, J_2 phase diagram are clearly inconsistent with experiment; see Supplementary Discussion 2 and Supplementary Fig. 3.) We proceed to show that the discrepancy in peak widths can be accounted for by considering finite-temperature effects in the XY model.

It has long been known that triangular XY magnets are thermally unstable to the formation of spin vortices, which act to broaden Bragg reflections in the corresponding magnetic scattering patterns[41]. These vortices are collective multi-spin objects that obey their own particular physics—for example, the so-called 'Kosterlitz–Thouless' transition that allows vortices to move throughout a lattice at elevated temperatures[42]. As in the magnetic skyrmion states of current interest in data storage applications, spin vortices carry topologically protected information in the form of their winding number, which may equal ±1 (ref. 43). Monte Carlo simulations of two-dimensional magnets are (in)famously sensitive to finite size effects[44,45], but we find that a simple quench Monte Carlo (QMC) protocol driven by equation (6) yields conveniently sized configurations capturing the two essential ingredients of interest to our current study, namely ferroquadrupolar order and spin vortices (Fig. 3e). We interpret these configurations as non-equilibrium approximations to the computationally inaccessible finite-temperature equilibrium spin structure. The corresponding structural models for $Au_{1/2}Ag_{1/2}(CN)$, as represented in Fig. 3f, finally yield an X-ray diffraction pattern with the correct variation in both intensity and peak widths (Fig. 3b and Supplementary Fig. 4). Consequently, we can be confident that this supramolecular analogue of the triangular XY ferroquadrupolar phase—the first model ever to reproduce the experimental diffraction pattern[27]—captures the key structural features of $Au_{1/2}Ag_{1/2}(CN)$. The subtleties in energy profile corresponding to

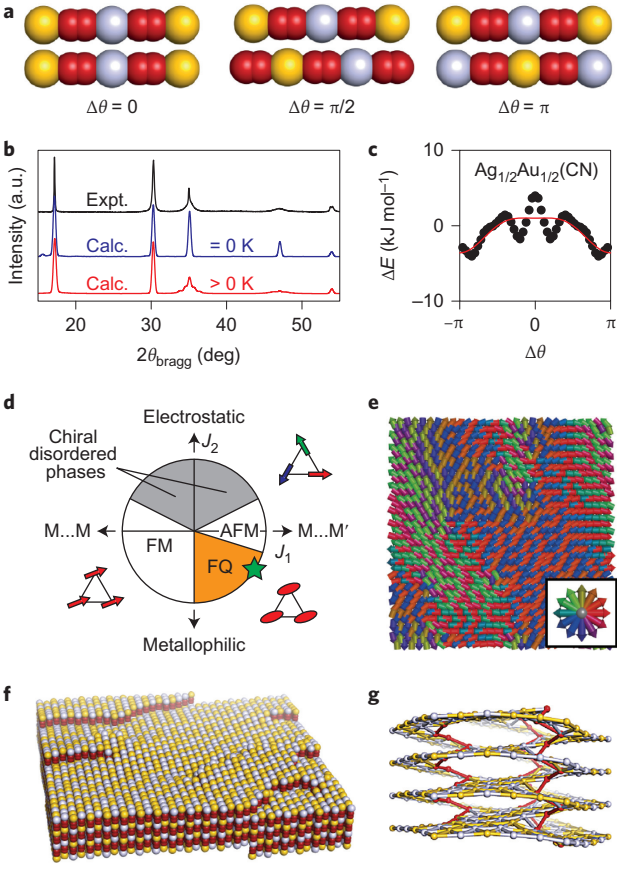

Figure 3 | Interactions and structural complexity in $Au_{1/2}Ag_{1/2}(CN)$. **a**, The metal–cyanide chains now consist of strictly alternating Au–CN–Ag–NC–Au linkages (Au atoms, yellow; Ag atoms, grey; cyanide ions, red). **b**, Comparison of the experimental X-ray diffraction pattern (Cu Kα radiation) of $Au_{1/2}Ag_{1/2}(CN)$[27] (indexing as for AuCN) with that calculated for the ground-state (blue) and finite-temperature (red) models described in the text. Our measurements gave an identical pattern (Supplementary Fig. 1). **c**, Interaction potential calculated for a pair of $Au_{1/2}Ag_{1/2}(CN)$ chains as a function of phase shift $\Delta\theta$ (data, filled circles; second-order Fourier fit, red line). **d**, Equilibrium phase diagram for the BLBQ triangular XY model, showing stability regions for ferromagnetic (FM; all spins aligned), antiferromagnetic (AFM; neighbouring spins reoriented by 120°), ferroquadrupolar (FQ; all spins aligned along a common axis, represented here by ovals) and chiral disordered phases[6]. The fitted parameters J_1, J_2 are marked by a green star and lie within the FQ domain, where spins align along a common axis but have no dipolar order. M and M′ are Ag or Au, indicating the preference for homometallic or heterometallic interactions. **e**, Representative QMC spin configuration; different colours correspond to different spin orientations (inset). FQ order is evident in the existence of stripes. **f**, Structural model for $Au_{1/2}Ag_{1/2}(CN)$ generated from the spin configuration shown in **e**. Note the absence of Au/Ag order within the metal-containing layers. **g**, A section of the same model, with C and N atoms omitted and three screw dislocations highlighted in red.

higher-order Fourier terms (Fig. 3c) will probably result in small additional modulations of the metallophilic layers, but these are not required to account for the diffraction behaviour. Our mapping between spin states and chain configurations has translated spin vortices into screw dislocations, which have become the topologically protected collective objects responsible for the experimentally observed selective peak broadening (Fig. 3f). Moreover, what our analysis implies is that these emergent multi-chain entities are actually encoded for by the self-interaction potential of an individual –Au–CN–Ag–NC–Au– chain. Looking further ahead, this link between individual chemical component and large-scale

topological defect suggests a broader supramolecular strategy for engineering complex materials; for example, the controlled incorporation of screw dislocations as a means of tuning the electronic band structure of topological insulators[46].

Conclusions. We have established an analogy between the structural frustration of gold(I) and/or silver(I) cyanide coordination polymers and the spin frustration of triangular XY magnets. Although we have focused on interpreting the structural consequences of this mapping between supramolecular and magnetic interactions, there is of course scope for drawing parallels between excitations and/or the response to external stimuli (T, p, H and so on) of both systems[47]. Are the screw dislocations we observe pinned or mobile, for example? Can temperature or pressure be used to vary the relative strengths of the different exchange parameters? There is cause here for optimism: a preliminary investigation of the high-pressure behaviour of AgCN suggests a sluggish transformation to a AuCN-structured polymorph that might be rationalized in terms of a change in sign of J_{eff} as argentophilic interaction energies increase more rapidly with decreasing interchain separation (r) than the electrostatic contribution (proportional to r^{-6} versus r^{-1}; Supplementary Discussion 3 and Supplementary Figs 5 and 6)[32]. Given the especially delicate balance of competing energy terms in $Au_{1/2}Ag_{1/2}(CN)$ and the accessibility of extensive substitution chemistry for this system[27], variable-temperature/pressure studies of the heterometallic cyanides offer an especially attractive avenue of future research.

In general, one might expect that kinetics will play a greater role for supramolecular analogues of frustrated magnets than in the magnetic systems themselves, given that the effective exchange energies involved can be larger by one or two orders of magnitude. On the one hand, this has the likely advantage of stabilizing the most interesting phases to ambient conditions—crucial if topological states are actually to be employed in room-temperature data storage technology. On the other hand, the key disadvantage will be the difficulty in interpreting phase behaviour in terms of equilibrium models, which are arguably the mainstay of the field of frustrated magnetism. The presence of multiple local minima in the self-interaction potential (as in Fig. 3c) may add further complications. Similarly, finite-size effects may become important for nanocrystalline preparations. One way or the other, what we have demonstrated here is how the interaction potential encoded within a material fragment might be tuned chemically to give rise to a variety of supramolecular structures—both simple and complex—the nature of which can be reliably predicted by exploiting a mapping onto geometrically related problems in the seemingly unrelated field of frustrated magnetism.

Methods

Quantum mechanical calculations. Quantum chemical calculations were performed to measure the variations in enthalpy in pairs of metal cyanide chains as a function of phase shift $\Delta\theta$. For each system, two periodic chains were considered, with their equilibrium geometry and interchain distance fixed to the crystallographic values. The chains were then shifted by increments of 2° and for each value of the shift a single-point energy calculation was performed, resulting in $\Delta E(\Delta\theta)$ profiles. In the case of the homometallic AgCN and AuCN chains, where there is no order in the orientation of the cyanide ions, we used for the chains a repeating unit equal to four times the basic –M–(CN)– motif, to account for all four possible orientations of the two cyanide anions.

All calculations were performed in the density functional theory (DFT) approach with localized basis sets, using the CRYSTAL14 software[48]. We used all-electron Triple-Zeta Valence with Polarisation basis sets for C and N atoms[49], an energy-consistent relativistic 19-valence-electron pseudopotential and corresponding valence basis set for Ag[50] and an effective core potential for Au[51]. The shrinking factor of the reciprocal space net is set to 8, corresponding to 65 reciprocal space points at which the Hamiltonian matrix was diagonalized. The total energy obtained with this mesh is fully converged.

We used the *PBEsol0* global hybrid exchange–correlation functional[52,53]: of the exchange–correlation functionals benchmarked on the bulk structures of AgCN and AuCN, it gave the best agreement with experimental lattice parameters. Similarly, we investigated the effect of empirical dispersion corrections (in the Grimme scheme[54]) and showed that they did not change the conclusions reached (that is, the relative stability of the different structures studied). However, because the Ag–Ag and Au–Au interatomic distances in this study are close to the cutoff of the empirical correction, their inclusion might introduce non-physical behaviour in the energy profiles. As a consequence, all results presented here were obtained without any empirical correction for dispersion.

X-ray powder diffraction calculations. X-ray powder diffraction patterns were calculated using the CrystalDiffract software programme, using the unit cell parameters reported in ref. 27. Peak shapes were modelled using a Gaussian function with an empirically determined width of 0.4°. Corrections for preferred orientation were implemented, with the relevant parameters determined by inspection of the experimental data in ref. 27: a plate-like geometry was used for AuCN and $Au_{1/2}Ag_{1/2}(CN)$ patterns (alignment parameter 0.47) and a needle-like geometry was used for AgCN (alignment parameter 0.29).

Quench Monte Carlo simulations. A custom Monte Carlo code was used to generate spin configurations for subsequent mapping onto candidate $Au_{1/2}Ag_{1/2}(CN)$ structure models. The spin configurations consisted of a $30 \times 18 \times 1$ supercell of the orthorhombic setting of the triangular lattice (1,080 spins in total). The Monte Carlo energy term used to drive the simulation corresponded to equation (6). We used values of J_1 and J_2 given by our fits to the DFT self-interaction potential ($J_1 = +2.3(3)$ kJ mol^{-1}, $J_2 = -1.3(5)$ kJ mol^{-1}). Simulation progressed in two phases: a high-temperature regime ($T \gg J_i$) in order to allow initial randomization of spins, followed by a quench cool ($T \ll J_i$). Repeated simulations using this protocol reproduced qualitatively similar spin structures of the type shown in Fig. 3e. Analogous simulations using the full DFT self-interaction potential gave qualitatively similar configurations with higher defect concentrations (Supplementary Fig. 7).

Received 3 July 2015; accepted 18 January 2016; published online 22 February 2016

References

1. Nitschke, J. R. Systems chemistry: molecular networks come of age. *Nature* **462,** 736–738 (2009).
2. Tait, S. L. Surface chemistry: self-assembling Sierpiński triangles. *Nature Chem.* **7,** 370–371 (2015).
3. Sun, Q.-F. *et al.* Self-assembled $M_{24}L_{48}$ polyhedra and their sharp structural switch upon subtle ligand variation. *Science* **328,** 1144–1147 (2010).
4. Balazs, A. C. & Epstein, I. R. Chemistry. Emergent or just complex? *Science* **325,** 1632–1634 (2009).
5. Moessner, R. & Ramirez, A. P. Geometrical frustration. *Phys. Today* **59,** 24–29 (2006).
6. Žukovič, M. & Idogaki, T. Low-temperature long-range ordering of a classical *XY* spin system with bilinear-biquadratic exchange Hamiltonian. *Physica B* **329–333,** 1055–1056 (2003).
7. Anderson, P. W. Ordering and antiferromagnetism in ferrites. *Phys. Rev.* **102,** 1008–1013 (1956).
8. Harris, M. J., Bramwell, S. T., McMorrow, D. F., Zeiske, T. & Godfrey, K. W. Geometrical frustration in the ferromagnetic pyrochlore $Ho_2Ti_2O_7$. *Phys. Rev. Lett.* **79,** 2554–2557 (1997).
9. Bramwell, S. T. & Gingras, M. J. P. Spin ice state in frustrated magnetic pyrochlore materials. *Science* **294,** 1495–1501 (2001).
10. Pauling, L. The structure and entropy of ice and of other crystals with some randomness of atomic arrangement. *J. Am. Chem. Soc.* **57,** 2680–2684 (1935).
11. Castelnovo, C., Moessner, R. & Sondhi, S. L. Magnetic monopoles in spin ice. *Nature* **451,** 42–45 (2008).
12. Lacroix, C., Mendels, P. & Mila, F. *Introduction to Frustrated Magnetism* (Springer, 2011).
13. Ludlow, R. F. & Otto, S. Systems chemistry. *Chem. Soc. Rev.* **37,** 101–108 (2008).
14. Nagaosa, N. & Tokura, Y. Topological properties and dynamics of magnetic skyrmions. *Nature Nanotech.* **8,** 899–911 (2013).
15. Giblin, S. R., Bramwell, S. T., Holdsworth, P. C. W., Prabhakaran, D. & Terry, I. Creation and measurement of long-lived magnetic monopole currents in spin ice. *Nature Phys.* **7,** 252–258 (2011).
16. Nakatsuji, S. *et al.* Spin disorder on a triangular lattice. *Science* **309,** 1697–1700 (2005).
17. Blunt, M. O. *et al.* Random tiling and topological defects in a two-dimensional molecular network. *Science* **322,** 1077–1081 (2008).
18. Adamson, J., Funnell, N. P., Thompson, A. L. & Goodwin, A. L. Structural investigation of a hydrogen bond order–disorder transition in a polar one-dimensional confined ice. *Phys. Chem. Chem. Phys.* **16,** 2654–2659 (2014).
19. Simonov, A., Weber, T. & Steurer, W. Experimental uncertainties of three-dimensional pair distribution function investigations exemplified on the diffuse scattering from a tris-*tert*-butyl-1,3,5-benzene tricarboxamide single crystal. *J. Appl. Crystallogr.* **47,** 2011–2018 (2014).

20. Zeng, X. *et al.* Complex multicolor tilings and critical phenomena in tetraphilic liquid crystals. *Science* **331,** 1302–1306 (2011).
21. Shoemaker, D. P. *et al.* Atomic displacements in the charge ice pyrochlore $Bi_2Ti_2O_6O'$ studied by neutron total scattering. *Phys. Rev. B.* **81,** 144113 (2010).
22. Fairbank, V. E., Thompson, A. L., Cooper, R. I. & Goodwin, A. L. Charge-ice dynamics in the negative thermal expansion material $Cd(CN)_2$. *Phys. Rev. B* **86,** 104113 (2012).
23. Whitaker, M. J. & Greaves, C. Magnetic ordering in the pyrochlore Ho_2CrSbO_7 determined from neutron diffraction, and the magnetic properties of other RE_2CrSbO_7 phases (*RE*=Y, Tb, Dy, Er). *J. Solid State Chem.* **215,** 171–175 (2014).
24. Taroni, A. Artificial spin rotors. *Nature Mater.* **13,** 915 (2014).
25. Hibble, S. J., Cheyne, S. M., Hannon, A. C. & Eversfield, S. G. Beyond Bragg scattering: the structure of AgCN determined from total neutron diffraction. *Inorg. Chem.* **41,** 1042–1044 (2002).
26. Hibble, S. J., Hannon, A. C. & Cheyne, S. M. Structure of AuCN determined from total neutron diffraction. *Inorg. Chem.* **42,** 4724–4730 (2003).
27. Chippindale, A. M. *et al.* Mixed copper, silver, and gold cyanides, $(M_xM'_{1-x})CN$: tailoring chain structures to influence physical properties. *J. Am. Chem. Soc.* **134,** 16387–16400 (2012).
28. Sharpe, A. G. *The Chemistry of Cyano Complexes of the Transition Metals* (Academic, 1976).
29. Bowmaker, G. A., Kennedy, B. J. & Reid, J. C. Crystal structures of AuCN and AgCN and vibrational spectroscopic studies of AuCN, AgCN, and CuCN. *Inorg. Chem.* **37,** 3968–3974 (1998).
30. Jansen, M. Homoatomic d^{10}–d^{10} interactions: their effects on structure and chemical and physical properties. *Angew. Chem. Int. Ed. Engl.* **26,** 1098–1110 (1987).
31. O'Grady, E. & Kaltsoyannis, N. Does metallophilicity increase or decrease down group 11? Computational investigations of $[Cl–M–PH_3]_2$ (M=Cu, Ag, Au, [111]). *Phys. Chem. Chem. Phys.* **6,** 680–687 (2004).
32. Schmidbaur, H. & Schier, A. Argentophilic interactions. *Angew. Chem. Int. Ed.* **54,** 746–784 (2015).
33. Pyykkö, P. Theoretical chemistry of gold. *Angew. Chem. Int. Ed.* **43,** 4412–4456 (2004).
34. Tissier, M., Delmaotte, B. & Mouhanna, D. *XY* frustrated systems: continuous exponents in discontinuous phase transitions. *Phys. Rev. B* **67,** 134422 (2003).
35. Okumura, S., Yoshino, H. & Kawamura, H. Spin-chirality decoupling and critical properties of a two-dimensional fully frustrated *XY* model. *Phys. Rev. B* **83,** 094429 (2011).
36. Collins, M. F. & Petrenko, O. A. Triangular antiferromagnets. *Can. J. Phys.* **75,** 605–655 (1997).
37. Keen, D. A. & Goodwin, A. L. The crystallography of correlated disorder. *Nature* **521,** 303–309 (2015).
38. Laüchli, A., Mila, F. & Penk, K. Quadrupolar phases of the $S = 1$ bilinear-biquadratic Heisenberg model on the triangular lattice. *Phys. Rev. Lett.* **97,** 087205 (2006).
39. Qi, K., Qin, M. H., Jia, X. T. & Liu, J.-M. Phase diagram of ferromagnetic *XY* model with nematic coupling on a triangular lattice. *J. Magn. Magn. Mater.* **340,** 127–130 (2013).
40. Stoudenmire, E. M. & Trebst, S. & Balents, L. Quadrupolar correlations and spin freezing in *S*=1 triangular lattice antiferromagnets. *Phys. Rev. B* **79,** 214436 (2009).
41. Mermin, N. D. & Wagner, H. Absence of ferromagnetism or antiferromagnetism in one- or two-dimensional isotropic Heisenberg models. *Phys. Rev. Lett.* **17,** 1133–1136 (1966).
42. Kosterlitz, J. M. & Thouless, D. J. Ordering, metastability and phase transitions in two-dimensional systems. *J. Phys. C* **6,** 1181–1203 (1973).
43. Mühlbauer, S. *et al.* Skyrmion lattice in a chiral magnet. *Science* **323,** 915–919 (2009).
44. Falo, F., Floria, L. M. & Navarro, R. Monte Carlo simulations of finite-size effects in Kosterlitz Thouless systems. *J. Phys. Condens. Matter* **1,** 5139–5150 (1989).
45. Xu, H.-J. & Southern, B. W. Phase transitions in the classical *XY* antiferromagnet on the triangular lattice. *J. Phys. A* **29,** L133–L139 (1996).
46. Ran, Y., Zhang, Y. & Vishwanath, A. One-dimensional topologically protected modes in topological insulators with lattice dislocations. *Nature Phys.* **5,** 298–303 (2009).
47. Coudert, F.-X. Responsive metal–organic frameworks and framework materials: under pressure, taking the heat, in the spotlight, with friends. *Chem. Mater.* **27,** 1905–1916 (2015).
48. Dovesi, R. *et al.* CRYSTAL: a computational tool for the *ab initio* study of the electronic properties of crystals. *Z. Krist.* **220,** 571–573 (2005).
49. Peintinger, M. F., Oliveira, D. V. & Bredow, T. Consistent Gaussian basis sets of triple-zeta valence with polarization quality for solid-state calculations. *J. Comput. Chem.* **34,** 451–459 (2013).
50. Doll, K., Pyykkö, P. & Stoll, H. Closed-shell interaction in silver and gold chlorides. *J. Chem. Phys.* **109,** 2339–2345 (1998).
51. Hay, P. J. & Wadt, W. R. *Ab initio* effective core potentials for molecular calculations. Potentials for K to Au including the outermost core orbitals. *J. Chem. Phys.* **82,** 299–310 (1985).
52. Adamo, C. & Barone, V. Toward reliable density functional methods without adjustable parameters: The PBE0 model. *J. Chem. Phys.* **110,** 6158–6170 (1999).
53. Perdew, J. P. *et al.* Restoring the density-gradient expansion for exchange in solids and surfaces. *Phys. Rev. Lett.* **102,** 039902 (2009).
54. Grimme, S. Semiempirical GGA-type density functional constructed with a long-range dispersion correction. *J. Comput. Chem.* **27,** 1787–1799 (2006).

Acknowledgements

A.B.C., M.J.C., J.A.M.P. and A.L.G. acknowledge financial support from the Engineering and Physical Sciences Research Council (EPSRC; EP/G004528/2), the Science and Technology Facilities Council (STFC) and the European Research Council (ERC; grant ref: 279705). High-pressure synchrotron X-ray powder diffraction measurements were carried out at the I15 Beamline, Diamond Light Source, UK. Quantum chemistry calculations made use of high performance computing resources from GENCI (grant x2015087069).

Author contributions

A.B.C., M.J.C., J.A.M.P., F.-X.C. and A.L.G. conceived and designed the study. A.B.C., D.D. and M.G.T. performed the experiments. A.B.C., M.J.C., J.A.M.P. and A.L.G. interpreted the experimental data. F.-X.C. performed and interpreted the quantum chemistry calculations. A.L.G. wrote the paper. All authors discussed and commented on the manuscript.

Additional information

Supplementary information is available in the online version of the paper. Reprints and permissions information is available online at www.nature.com/reprints. Correspondence and requests for materials should be addressed to F.X.C. and A.L.G.

Competing financial interests

The authors declare no competing financial interests.